XI International Conference on Computational Plasticity. Fundamentals and Applications
COMPLAS XI
E. Oñate, D.R.J. Owen, D. Peric and B. Suárez (Eds)

RELATIONSHIP BETWEEN DEFORMATION AND STABILITY SWITCHING IN AMORPHOUS METAL : LOCAL LATTICE INSTABILITY ANALYSIS

MASAOMI NISHIMURA*, KISARAGI YASHIRO† AND MASAHIRO ARAI‡

*,‡Department of Mechanical Systems Engineering, Shinsyu University
Wakasato 4-17-1, Nagano 380-8553, Japan
e-mail: nishimu@shinshu-u.ac.jp, http://str.shinshu-u.ac.jp
e-mail: arai@shinshu-u.ac.jp, http://str.shinshu-u.ac.jp

†Graduate School of Engineering, Kobe University
Rokkodai 1-1, Nadaku, Kobe 657-8501, Japan
e-mail: yashiro@mech.kobe-u.ac.jp, http://mm4.scitec.kobe-u.ac.jp

Key words: Molecular Dynamics Simulation, Amorphous Metals, Local Lattice Instability Analysis, Stability-Switching, Local Volume Change

Abstract. We have attempted to comprehend the deformation behavior of amorphous metals by the local lattice instability analysis that discusses the positiveness of atomic elastic stiffness coefficients, B_{ij}^{α}, or the second-order derivatives of atomic energy composition. In the present study, we discuss the stability-switching, or transitions between $\det B_{ij}^{\alpha} \geq 0$ and $\det B_{ij}^{\alpha} < 0$, by the "probabilistic" fluctuation and the "deterministic" mechanical load. No-load equilibrium, tension, compression and simple shear are performed on an amorphous nickel by molecular dynamics simulations. The positive and negative stability-switching, or "stabilization" and "destabilization", occur due to the "probabilistic" fluctuation even at the equilibrium state. The number of $\det B_{ij}^{\alpha} < 0$ atoms shows almost constant while the distribution of $\det B_{ij}^{\alpha} < 0$ atoms indicates different morphology at each observation time. Ratios of switched atoms with stability-switching under tension, compression and shear are larger than that under the equilibrium because the local structural relaxation produces simultaneously both positive and negative stability-switching. Atoms with negative and positive stability-switching show increases and decreases of atomic volume, respectively; while only positive switching shows the decreases in local volumes, evaluated with the atomic volumes of surrounding atoms within the cutoff radius, according to the incidence of "deterministic" structural changes.

1 INTRODUCTION

Amorphous metals have short and middle range order such as an icosahedral atomic-cluster [1, 2]. These atomic scale structures play important roles in the formability and deformability of amorphous metals. On the other hand, it is difficult to understand universally deformation behaviors of these in disordered or inhomogeneous structure. We have discussed the mechanical characteristic of local structure by local lattice instability analysis (LLIA) [3] in molecular dynamics (MD) simulations. LLIA is expected to extract the universal mechanism of deformation because the local stability on LLIA is consistently determined only by the positive definiteness of atomic elastic stiffness coefficients, B^{α}_{ij}.

We have so far shown that amorphous metals have many $\det B^{\alpha}_{ij} < 0$ atoms even at the equilibrium state [4, 5] by LLIA. In our previous report [5], we have discussed the changes in $\det B^{\alpha}_{ij} < 0$ atoms in monatomic amorphous metals during uniaxial tension. Under the tension, it is considered from the comparison of stress components on $\det B^{\alpha}_{ij} \geq 0$ and $\det B^{\alpha}_{ij} < 0$ atoms that the local stress reduction occurs by transitions between each other. Then we have picked up atoms that have actually switched between $\det B^{\alpha}_{ij} \geq 0$ and $\det B^{\alpha}_{ij} < 0$. As a result, we have concluded that the stress relaxation is not caused by a straightforward image of "stabilization" or "destabilization", but by "shuffle of atomic arrangement" which involves positive and negative stability-switching.

In the present study, we perform compression and simple shear in addition to tension. In order to explore further relationship between deformation and the stability-switching based on LLIA in amorphous metals, we discuss the stability-switching by the "probabilistic" fluctuation and the "deterministic" mechanical load, and evaluate the changes of atomic and local volume on the stability-switching.

2 LOCAL LATTICE INSTABILITY ANALYSIS

Wang et al. have proposed the evaluation of lattice stability at finite strain and temperature, on the basis of the positive definiteness of elastic stiffness coefficients [6, 7]. The elastic stiffness, or stress-strain, coefficients are written as [8]

$$B_{ijkl} \equiv \left(\frac{\partial \sigma_{ij}}{\partial \varepsilon_{kl}}\right) = C_{ijkl} + \frac{1}{2}(\sigma_{il}\delta_{jk} + \sigma_{jl}\delta_{ik} + \sigma_{ik}\delta_{jl} + \sigma_{jk}\delta_{il} - 2\sigma_{ij}\delta_{kl}), \tag{1}$$

where δ_{ij} is Kronecker's delta. The stress, σ_{ij}, and the elastic coefficients, C_{ijkl}, are defined as

$$\sigma_{ij} = \frac{1}{V}\left(\frac{\partial U}{\partial \eta_{ij}}\right), \; C_{ijkl} = \frac{1}{V}\left(\frac{\partial^2 U}{\partial \eta_{ij}\partial \eta_{kl}}\right). \tag{2}$$

Here U is the internal energy and V is the volume of crystal at the equilibrium. Note that the differentiation in Eq. (2) is for the infinitesimal virtual strain, η_{ij}, at the equilibrium state under the external load. The B_{ijkl} combines the stress and actual strain, ε_{ij}, from the load-free reference state. In the linear elasticity region, B_{ijkl} is identical to C_{ijkl}

but it is not equivalent in the nonlinear elasticity or finite strain region. That is, B_{ijkl} represents the gradient at the stress-strain surface in the six dimensional strain spaces, whether the system is in the linear or nonlinear elasticity. Thus we can easily imagine the physical meaning of the Wang's stability criteria; it is the point where the crystal loses the deformation resistance. The symmetric part of the tensor of Eq. (1), $B_{ijkl}^{\mathrm{sym}} \equiv (B_{ijkl} + B_{lkji})/2$, dominates the lattice stability [6, 7]. The symmetric tensor B_{ijkl}^{sym} is represented by the 6×6 matrix, B_{ij} $(i, j = 1 \sim 6)$, in the Voigt notation [8]. Thus the instability criterion could be written as $\mathrm{det}B_{ij} < 0$.

The system energy, E_{tot}, can be divided into the contribution of each atom, E_α, in the framework of the embedded atom method (EAM) [9]. The atomic stress, σ_{ij}^α, and the atomic elastic coefficient, C_{ijkl}^α, are defined as the 1st and 2nd order derivatives of E_α against local strain perturbation, respectively. Thus, we can calculate the atomic elastic stiffness coefficients, B_{ijkl}^α, at any time and configuration in the MD simulation, using Eq.(1). The symmetric part of B_{ijkl}^α is also used for stability analysis, so that we denote the local instability condition as $\mathrm{det}B_{ij}^\alpha < 0$ $(i, j = 1 \sim 6)$, according to the Voigt notation.

3 SIMULATION PROCEDURE

An amorphous nickel is made by usual melt-quench simulation under the periodic boundary condition in all directions. The interatomic potential adopted is the EAM by Voter and Chen [10]. The total number of atoms is 108,000. A nickel crystal is melted during 10ps MD calculation at the temperature of $T = 3000$K. The temperature is quenched to 10K with the cooling rate of -5×10^{13}K/s. The no-load calculation is performed during 200ps at $T = 10$K after the melt-quench simulation. Then, tension, compression and simple shear are applied on the amorphous nickel under the periodic boundary. The tension or compression is performed by uniform expansion or contraction of the distance of each atom in the z-direction. The strain rates of tension and compression are 1.0×10^8/s. The cell length in the transverse directions is also controlled to cancel the normal stress originated by the Poisson's contraction/expansion. On the other hand, simple shear is performed by transition from the cubic cell to the monoclinic one. The cell length of x and y direction are fixed; and the system volume is unchanged during the shear deformation. The strain rate is also set to 1.0×10^8/s in engineering strain. The temperature is kept at 10K by velocity scaling during all the deformations.

4 RESULTS AND DISCUSSION

4.1 No-load calculation

Figure 1 shows a change in a potential energy during no-load calculation after the melt-quench simulation. The potential energy drastically decreases on the initial stage of the calculation because the structural relaxation continues from the melt-quench simulation. The decrease stops at 50ps, while there is a slight plateau of energy from 20ps to 30ps.

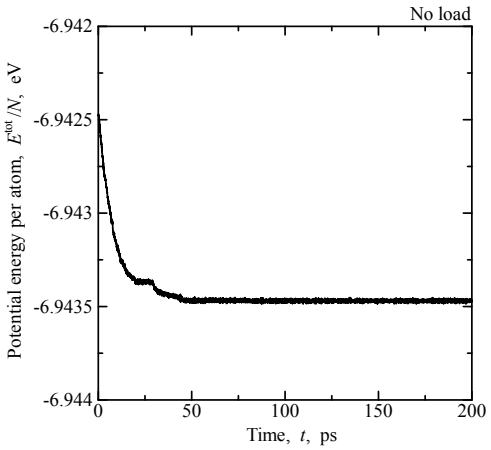

Figure 1: Change in the potential energy during the no-load calculation.

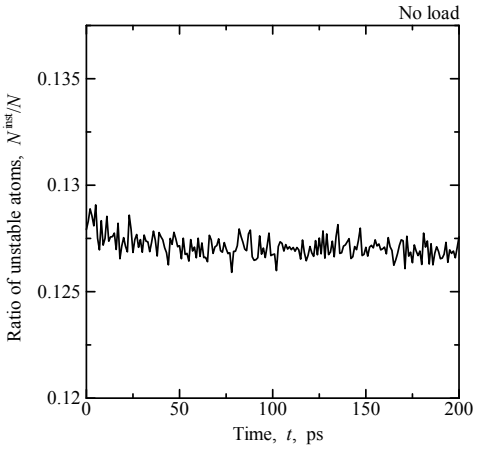

Figure 2: Change in the ratio of $\det B_{ij}^{\alpha} < 0$ atoms during the no-load calculation.

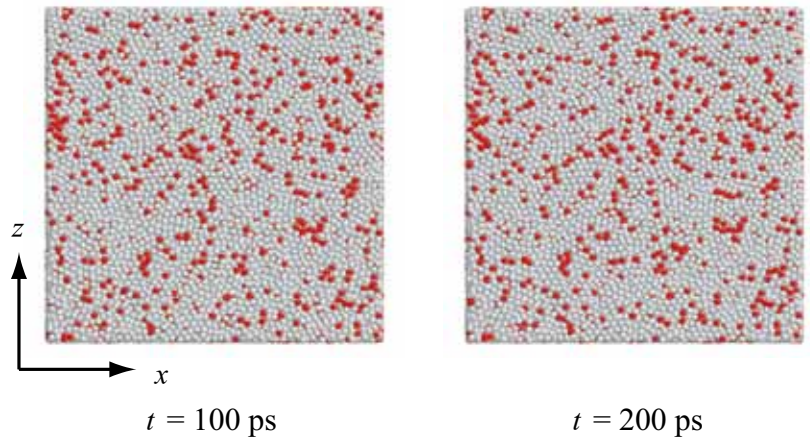

Figure 3: Distributions of $\det B_{ij}^{\alpha} < 0$ atoms at $t = 100$ps and 200ps in the no-load calculation.

This change is caused by the nucleation of a fractional crystalline structure; only 0.1% atoms are evaluated as "crystal" by this change. The potential energy remains unchanged after 50ps. Thus, the amorphous nickel has reached an equilibrium state.

Figure 2 shows a change in the ratio of $\det B_{ij}^{\alpha} < 0$ atoms during the no-load calculation. We have evaluated the elastic stiffness coefficient, B_{ij}^{α}, of all atoms on each 1ps. N^{inst}/N is "momentary" ratio of $\det B_{ij}^{\alpha} < 0$ atoms, where N^{inst} and N are a number of $\det B_{ij}^{\alpha} < 0$ atoms and a total number of atoms, respectively. N^{inst}/N slightly decreases from 0ps to 20ps on the initial stage, while there is no change of N^{inst}/N by the nucleation of a crystalline structure. The ratio of $\det B_{ij}^{\alpha} < 0$ atoms seems mostly unchanged and vibrates at around 12.7% during the energy equilibrium after 50ps. Thus, the amorphous nickel contains many "unstable" atoms of $\det B_{ij}^{\alpha} < 0$ even in the no-load equilibrium, and the ratio is almost constant. Figure 3 shows snapshots of the amorphous nickel at $t = 100$ps

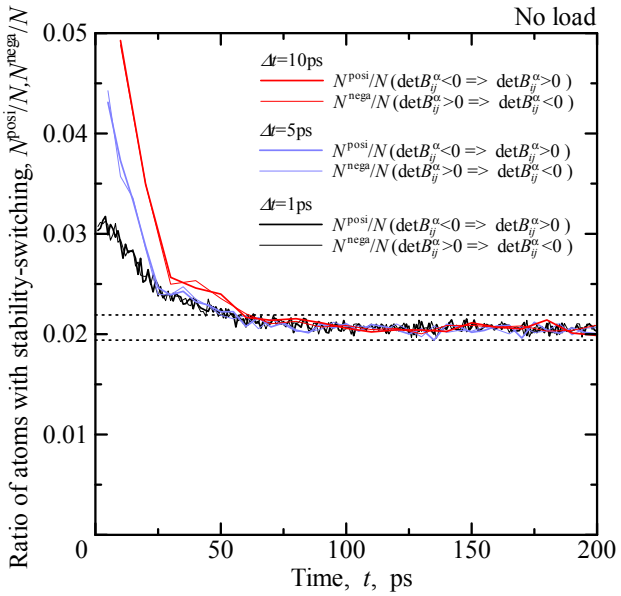

Figure 4: Changes in the ratio of atoms that have switched their stability for Δt in the no-load calculation.

and 200ps. Distributions of $\mathrm{det}B_{ij}^{\alpha} < 0$ atoms are indicated by red circles. There is no difference between atomic structure of Fig.3(a) and (b) because this amorphous metal has achieved equilibrium from $t = 50$ps. On the other hand, we can find a difference in the distribution of $\mathrm{det}B_{ij}^{\alpha} < 0$ or red atoms. That is, although the ratio of $\mathrm{det}B_{ij}^{\alpha} < 0$ atoms is almost constant in Fig.2, it is not always true that the distribution of $\mathrm{det}B_{ij}^{\alpha} < 0$ is same. We can understand that the stability-switching such as $\mathrm{det}B_{ij}^{\alpha} \geq 0 \leftrightarrow \mathrm{det}\ B_{ij}^{\alpha} < 0$ occurs even in the equilibrium state.

Then we have picked up atoms that have actually switched between $\mathrm{det}B_{ij}^{\alpha} \geq 0$ and $\mathrm{det}B_{ij}^{\alpha} < 0$ for each time interval of Δt. Figure 4 shows changes in ratios of these atoms, where N^{posi}/N and N^{nega}/N are the ratio of atoms with the positive change from $\mathrm{det}B_{ij}^{\alpha} < 0$ to $\mathrm{det}B_{ij}^{\alpha} \geq 0$ and the negative change from $\mathrm{det}B_{ij}^{\alpha} \geq 0$ to $\mathrm{det}B_{ij}^{\alpha} < 0$, respectively. We have evaluated the stability-switching by comparing of "momentary" values of $\mathrm{det}B_{ij}^{\alpha}$ before and after time intervals as Δt =1ps, 5ps or 10ps. N^{posi}/N shown with heavy lines and N^{nega}/N shown with thin lines are almost the same path. At the initial stage of relaxation before $t = 50$ps, ratios of N^{posi} and N^{nega} decrease and its decrease rate varies according to the evaluation time interval. This difference by the time interval disappears at 70ps. Moreover, all the ratios of N^{posi} and N^{nega} converges with 2.0% after 70ps. Two horizontal dotted lines describe upper and lower limits of the stability-switching after 70ps. We can understand that these ratios of stability-switching are caused by the "probabilistic" fluctuation such as the subtle change in local mechanical condition by the atomic perturbation or thermal vibration. Under the non-equilibrium state before 70ps, N^{posi}/N and N^{nega}/N show higher value than the upper limits under the equilibrium,

and vary according to the time interval because one-way stability-switching caused by "deterministic" nonequilibrium change is added to the ratio of the "probabilistic" changes.

4.2 Tension, compression and shear

Figure 5 shows stress-strain curves and changes in the ratio of $\det B_{ij}^{\alpha} < 0$ atoms under the tension, compression and shear. The scale of stress is indicated in the right axis. Stress and strain in the compression are shown by absolute value for comparison. Stresses show linear increases on the initial stage in every deformation. Gradients of stress-strain curves in the tension and compression are almost the same. After the linear increase, stress-strain curves become nonlinear, and alternate between increase and decrease showing zigzag response. We have evaluated $\det B_{ij}^{\alpha} < 0$ of all atoms at each 5ps, which correspond to the strain of 0.0005. Ratios of these atoms, N^{inst}/N, show the increasing tendency in every deformations. On the other hand, the ratio in tension shows a peak around $\varepsilon_{zz} = 0.037$ shown with a vertical broken line in Fig.5(a).

Figure 6 indicates the changes in the ratio of atoms that show stability-switching. As shown in Fig.4, we investigate the switching of positiveness of $\det B_{ij}^{\alpha}$ for several time intervals. In this figure, $\Delta t = 5$ps and 10ps, or $\Delta\varepsilon_{zz}, \Delta\gamma_{zx} = 0.0005$ and 0.001, are selected as intervals for comparison of $\det B_{ij}^{\alpha}$. Stress-strain curves are also shown. Horizontal dotted lines describe upper and lower limit of the stability-switching under the equilibrium state (Fig.4). Changes in N^{posi}/N and N^{nega}/N are shown by heavy lines and thin ones, respectively; while they are almost same just like in the no-load calculation of Fig.4. However, note that the accumulation of slight difference between them leads increase of $\det B_{ij}^{\alpha} < 0$ atoms under deformations (Fig.5). N^{posi}/N and N^{nega}/N stay in the upper and lower zone of equilibrium state in the initial stage. Then, they jump up from the upper limits around vertical dash-dotted lines shown with (A), and vary according to the time interval. These strains correspond with transition points from linear to nonlinear on stress-strain curves. After these strain, the tension and compression show larger ratios of stability-switching than the upper limit of equilibrium state. On the other hand, the ratios under the shear sometimes return to ratio zone of the equilibrium state. The N^{posi}/N and N^{nega}/N jump up again from the upper limits at vertical dash-dotted lines in Fig.6(c). The gradient of stress-strain curve also changes at these points. If we assume the ratio of "probabilistic" stability-switching is not changed under the deformation, the increase beyond the upper dotted line suggests the incidence of "deterministic" stability-switching by structural changes such as collapses of atomic cluster shown in our previous report [4]. In addition, occurrences of "deterministic" structural change induce differences of stability-switching according to time intervals, as shown in the non-equilibrium of Fig.4. In tension and compression of Figs. 6(a) and (b), the difference by time intervals after (A) almost disappear at vertical dash-dotted lines. Gradients of stress-strain curves also change at these lines. These suggest that the stress relaxation is caused by "shuffle of atomic arrangement" which involves positive and negative stability-switching simultaneously. Vertical dashed lines indicate the remarkable peak of N^{posi}/N and N^{nega}/N. These

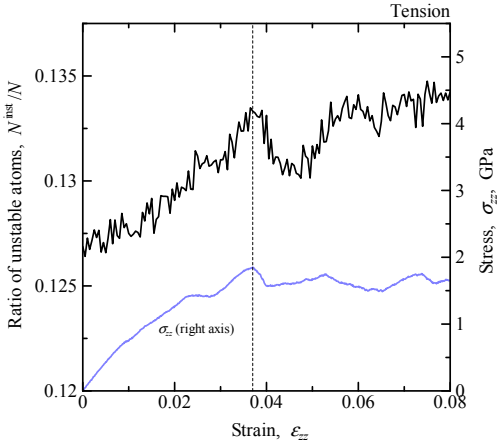

(a) Tension

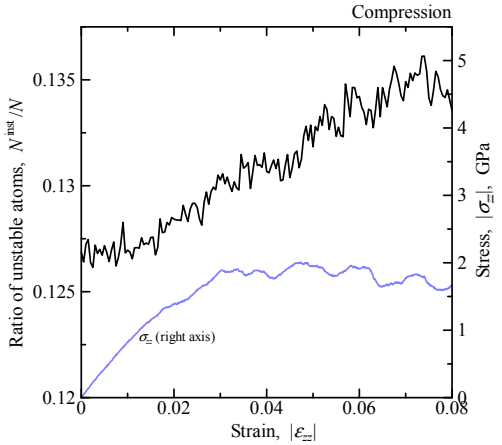

(b) Compression

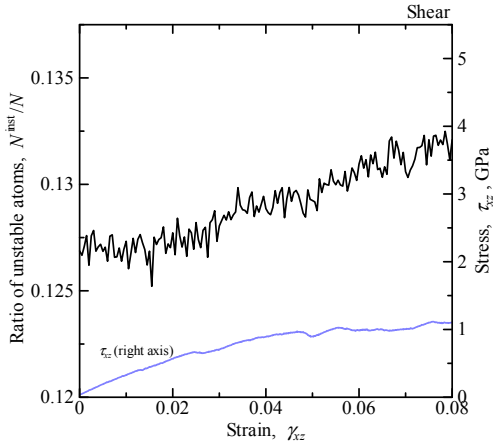

(c) Shear

Figure 5: Changes in the ratio of $\det B_{ij}^{\alpha} < 0$ atoms and stress-strain curves under the tension, compression and shear.

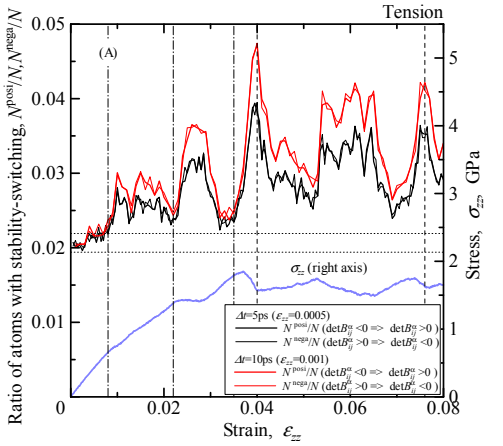

(a) Tension

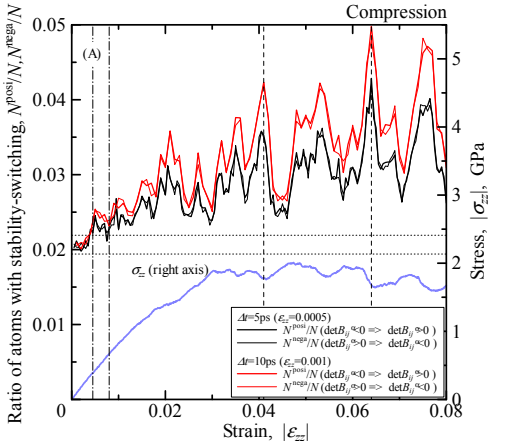

(b) Compression

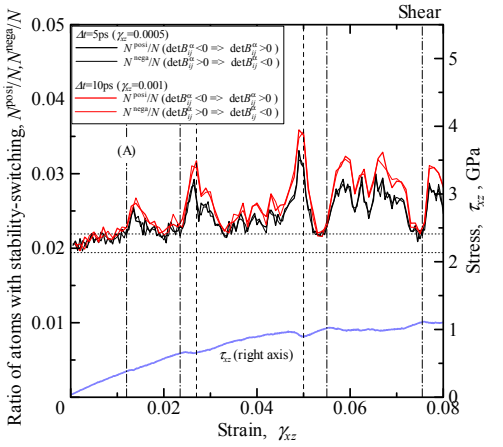

(c) Shear

Figure 6: Changes in the ratio of atoms that have switched their stability for Δt and stress-strain curves under the tension, compression and shear.

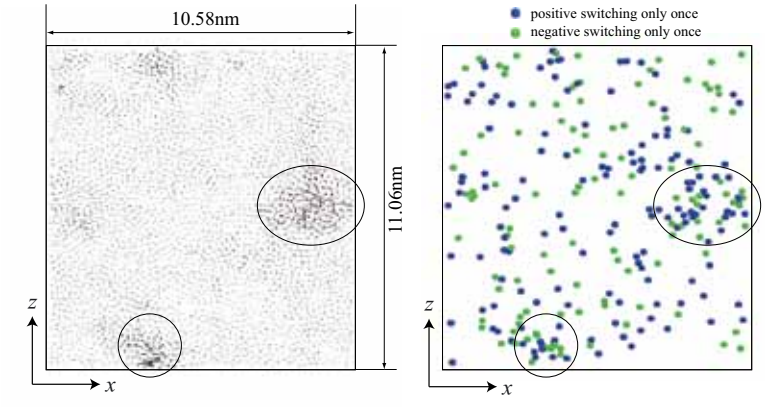

(a) Displacements of atoms (b) The distribution of atoms that have switched between stable and unstable

Figure 7: Comparison between atom motions and distribution of atoms that have switched their stability during $\varepsilon_{zz} = 0.035 \sim 0.037$ under tension.

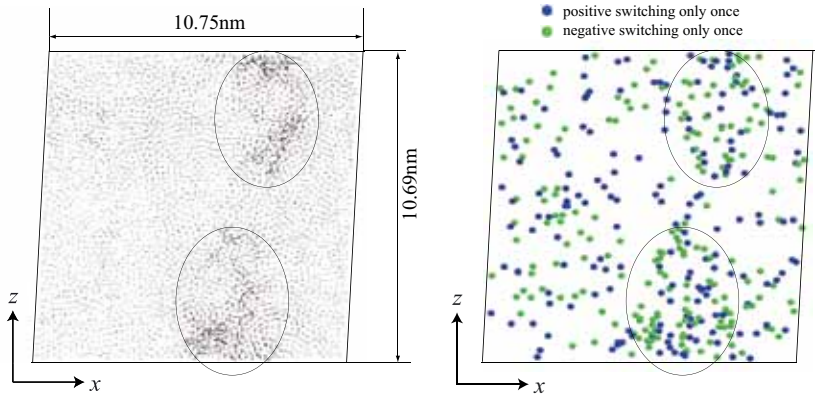

(a) Displacements of atoms (b) The distribution of atoms that have switched between stable and unstable

Figure 8: Comparison between atom motions and distribution of atoms that have switched their stability during $\gamma_{xz} = 0.05 \sim 0.052$ under shear.

correspond with the valley of stress-strain curves because stress relaxations weaken due to reduction of the shuffles.

We have considered a relationship between the local deformation and the stability-switching. Figures 7 and 8 show (a) the magnitude and direction of migration of each atoms with small vector and (b) the distribution of atoms that have switched between $\det B_{ij}^{\alpha} \geq 0$ and $\det B_{ij}^{\alpha} < 0$, during $\varepsilon_{zz} = 0.035 \sim 0.037$ in the tension and $\gamma_{xz} = 0.055 \sim 0.056$ in the shear, respectively. These periods just correspond to spans from the onset point of the increment of N^{posi} and N^{nega}, as shown with vertical dash-dotted lines in Fig.6, to the peak points of stress-strain curves. The trajectory and distribution

are shown only thin part in the simulation cell, in which the atoms show the largest migration during these periods. Colored circles in Figs.7(b) and 8(b) are atoms with stability-switching only once for each strain interval of 0.0005 during these observation periods; green atoms have negatively switched and blue ones have positively done. Some atoms switch their stabilities more than once, but these are mainly caused by probabilistic changes. Thus, these atoms are not shown in Figs.7(b) and 8(b) because we want to understand the relationship between the local deformation and the stability switching. We can find remarkable atom rearrangements as shown with ellipsoids in Figs.7(a) and 8(a). These regions have many atoms with stability-switching in Figs.7(b) and 8(b). This demonstrates that the "shuffle of atomic arrangement" simultaneously produce both positive and negative stability-switching. Note that these periods are before the peaks of stress-strain curves. The emergence of these local events leads to the global deformation. It is suggested the possibility that we can evaluate the origin of global deformation by the observation of the stability switching.

4.3 Volume changes by the stability-switching

In order to understand structural changes by the stability-switching, we evaluated a volume change of Voronoi polyhedron of each atom under tension, compression and shear. Voronoi polyhedra are determined by nearest neighbor atoms of center atom. Thus, we can regard the Voronoi volume, V_α, as an atomic volume of atom α. Variations of Voronoi volume by the stability-switching are determined as follows;

$$\Delta V_\alpha^{\mathrm{posi}} = \frac{1}{N^{\mathrm{posi}}} \sum_i^{N^{\mathrm{posi}}} \{V_i(t) - V_i(t-\Delta t) - \Delta V_\alpha^{\mathrm{all}}\},$$
$$\Delta V_\alpha^{\mathrm{nega}} = \frac{1}{N^{\mathrm{nega}}} \sum_i^{N^{\mathrm{nega}}} \{V_i(t) - V_i(t-\Delta t) - \Delta V_\alpha^{\mathrm{all}}\}, \tag{3}$$

where N^{posi} and N^{nega} are the number of atoms with positive and negative stability-switching for the time interval of Δt. $\Delta V_\alpha^{\mathrm{all}}$ is determined by a system volume, V, as

$$\Delta V_\alpha^{\mathrm{all}} = \frac{1}{N} \sum_i^N \{V_i(t) - V_i(t-\Delta t)\} = \frac{1}{N}\{V(t) - V(t-\Delta t)\}. \tag{4}$$

We uniformly remove the effect due to affine deformation from each atom because the system volume changes under the tension and compression. $\Delta V_\alpha^{\mathrm{all}}$ in the shear is zero, all of the time. Figure 9 shows changes in $\Delta V_\alpha^{\mathrm{posi}}$ and $\Delta V_\alpha^{\mathrm{nega}}$ under the tension, compression and shear. The interval for evaluation of stability-switching is $\Delta t = 10$ps, or $\varepsilon_{zz}, \gamma_{xz} = 0.001$. Vertical lines shown in Fig.6 are indicated again in this figure. Shapes of the changes in $\Delta V_\alpha^{\mathrm{nega}}$ are similar to those in the ratio of stability-switching previously shown in Fig.6, while $\Delta V_\alpha^{\mathrm{posi}}$ are opposite in sign to $\Delta V_\alpha^{\mathrm{nega}}$. So that, the volume increase and decrease are induced by the negative and positive stability-switching, respectively.

Magnitudes of $\Delta V_\alpha^{\rm posi}$ and $\Delta V_\alpha^{\rm nega}$ rise just behind vertical dash-dotted lines as shown by arrows, and peaks of these also correspond with dashed lines. It is suggested that the volume change by "deterministic" stability-switching are larger than that by "probabilistic" one. Volume changes of $\Delta V_\alpha^{\rm posi}$ and $\Delta V_\alpha^{\rm nega}$ almost get balanced out each other because ratios of $N^{\rm posi}$ and $N^{\rm nega}$ almost coincide with each other.

We can understand the volume change of an atom by the stability-switching. On the other hand, structural changes on the amorphous metal occur in dozens of atoms, as shown in Figs.7 and 8. We evaluate the changes in local volume around atoms with the stability-switching,

$$\Delta V_{\rm rc}^{\rm posi} = \frac{1}{N^{\rm posi}} \sum_i^{N^{\rm posi}} \sum_j^{N_i^{\rm rc}} \{V_j(t) - V_j(t-\Delta t) - \Delta V_\alpha^{\rm all}\}$$
$$\Delta V_{\rm rc}^{\rm nega} = \frac{1}{N^{\rm nega}} \sum_i^{N^{\rm nega}} \sum_j^{N_i^{\rm rc}} \{V_j(t) - V_j(t-\Delta t) - \Delta V_\alpha^{\rm all}\} \quad (5)$$

where $N_i^{\rm rc}$ is the number of atoms in a sphere centering on atom i at time of t. A radius of this sphere is 0.48nm, which correspond with a cutoff radius for calculation of EAM interaction. Thus, $\Delta V_{\rm rc}^{\rm posi}$ and $\Delta V_{\rm rc}^{\rm nega}$ mean volume changes of the spherical region around atoms with negative and positive stability-switching. Figure 10 shows changes in the $\Delta V_{\rm rc}^{\rm posi}$ and $\Delta V_{\rm rc}^{\rm nega}$ under the tension, compression and shear. $\Delta V_{\rm rc}^{\rm nega}$ has a tendency of volume increase, and $\Delta V_{\rm rc}^{\rm posi}$ do that of volume decrease; however, these are not symmetric about the x-axis. Values of $\Delta V_{\rm rc}^{\rm posi}$ exhibit a clear declining trend just behind vertical dash-dotted lines as shown by arrows, and almost peaks of these correspond with dashed lines. On the other hand, we cannot find clear correspondences between $\Delta V_\alpha^{\rm nega}$ and vertical lines. Here, these changes in $\Delta V_{\rm rc}^{\rm posi}$ are not caused by only an atomic volume change of the center atom. Note that scales of y-axis in Fig.10 are larger than those in Fig.9. Thus, the positive stability-switching, or "stabilization", produces a local volume decrease with surrounding neighbor atoms. Both positive and negative stability-switching under the deformations occur at the same region, as previously shown in Figs.7 and 8. Thus the negative stability-switching occurs in order to absorb the volume decrease by the stabilization.

5 CONCLUSIONS

In order to explore further relationship between deformation in amorphous metals and changes in the atomic stability determined by the positiveness of atomic elastic stiffness coefficients, B_{ij}^α, we have discussed stability-switching as $\det B_{ij}^\alpha < 0 \leftrightarrow \det B_{ij}^\alpha \geq 0$ in an amorphous nickel under several deformations. First, $\det B_{ij}^\alpha$ of all atoms are evaluated during the no-load calculation after the melt-quench simulation. The negative and positive stability-switching occur due to the "probabilistic" fluctuation even at the equilibrium state, and the number of $\det B_{ij}^\alpha < 0$ atoms shows almost constant while the distribution

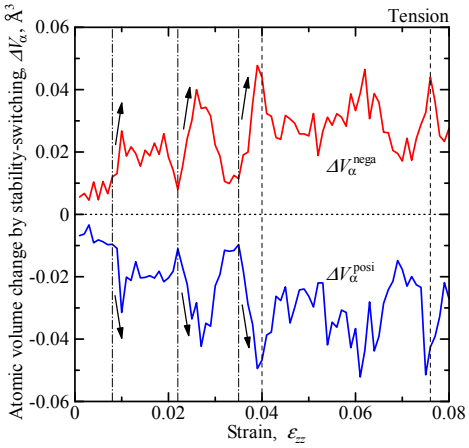

(a) Tension

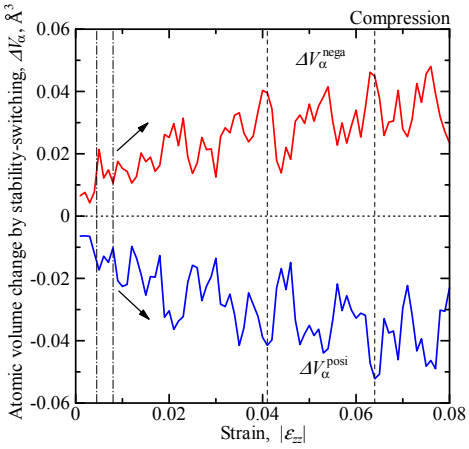

(b) Compression

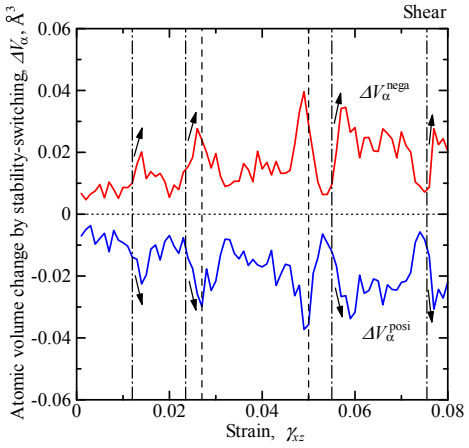

(c) Shear

Figure 9: Changes in variation of atomic volume by the stability-switching under the tension, compression and shear.

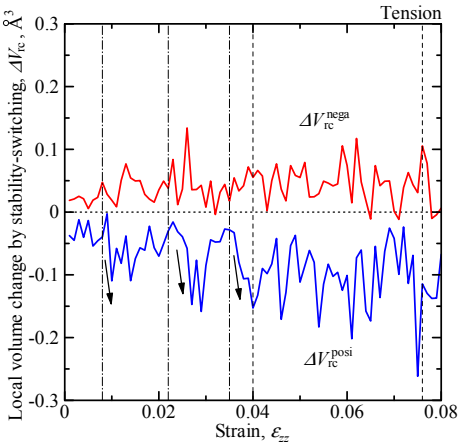

(a) Tension

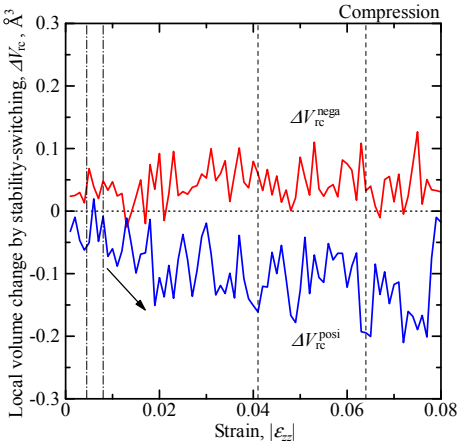

(b) Compression

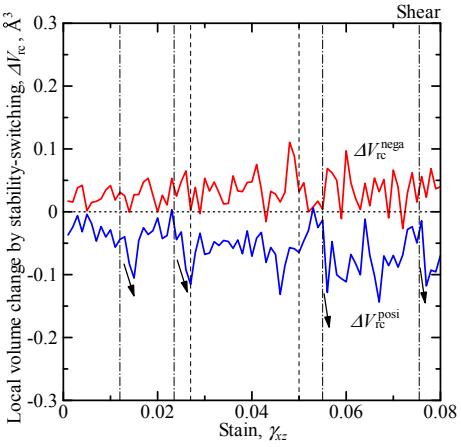

(c) Shear

Figure 10: Changes in variation of local volume by the stability-switching under the tension, compression and shear.

of $\det B_{ij}^{\alpha} < 0$ atoms changes from time to time. Then, tension, compression and simple shear are applied on the amorphous nickel in order to discuss the stability-switching by "deterministic" mechanical load. We have revealed the following facts : (1) The number of $\det B_{ij}^{\alpha} < 0$ atoms shows the increasing tendency under deformations. (2) Ratios of atoms with stability-switching under deformations is larger than that under the equilibrium because the local structural relaxation produces simultaneously both positive and negative stability-switching. (3) Atoms with negative and positive stability-switching show increases and decreases of atomic volume, respectively. Moreover, magnitude of both volume changes rise according to the incidence of "deterministic" stability-switching. (4) The negative and positive stability-switching also produce increases and decreases of local volume, evaluated with the atomic volumes of surrounding atoms within the cutoff radius, respectively; while only positive switching shows the correspondence between the change of local volume and the incidence of "deterministic" stability-switching.

REFERENCES

[1] M. Shimono and H. Onodera, Short-Range and Medium-Range Order in Supercooled Liquids of Alloys, *Mat. Sci. Eng. A* (2007) **449–451**:717–721.

[2] H. W. Sheng, W. K. Luo, F. M. Alamgir, J. M. Bai and E. Ma, Atomic Packing and Short-to-Medium-Range Order in Metallic Glasses, *Nature* (2006) **439**:419–425.

[3] K. Yashiro and Y. Tomita, Local lattice instability at a dislocation nucleation and motion, *J. de Phys. IV*(2001) **11**:Pr5-3-Pr5-10.

[4] K. Yashiro, M. Nishimura and Y. Tomita, Deformation analysis of amorphous metals based on atomic elastic stiffness coefficients, *Model. Sim. Mater. Sci. Eng.* (2006) **14**:597-605.

[5] M. Nishimura, K. Yashiro and M. Arai, Local lattice instability analysis on amorphous metals: switching between stable and unstable atoms, *J. Sol. Mech. Mater. Eng.* (2010) **4**:1550-1562.

[6] J. Wang, S. Yip, S. R. Phillpot and D. Wolf, Crystal instabilities at finite strain, *Phys. Rev. Lett.* (1993) **71**:4182–4185.

[7] J. Wang, J. Li, S. Yip, S. R. Phillpot and D. Wolf, Mechanical instabilities of homogeneous crystals, *Phys. Rev. B* (1995) **52**:12627–12635.

[8] P. C. Wallace, *Thermodynamics of Crystals*. Wiley, Newyork, (1972).

[9] M. S. Daw and M. I. Baskes, Embedded–Atom Method : Derivation and Application to Impurities, Surfaces and Other Defects in Metals, *Phys. Rev. B* (1984) **29**:6443–6453.

[10] A. F. Voter and S. P. Chen, Accurate Interatomic Potentials for Ni, Al and Ni_3Al, *Mater. Res. Soc. Sympo. Proc.* (1987) **82**:175-180.